









ORIGINAL ARTICLE

Plant, Cell & Environment

WILEY

Predicting biochemical acclimation of leaf photosynthesis in soybean under in-field canopy warming using hyperspectral reflectance

Etsushi Kumagai^{1,2}  | Charles H. Burroughs²  | Taylor L. Pederson^{2,3} | Christopher M. Montes²  | Bin Peng⁴  | Hyungsuk Kimm⁴  | Kaiyu Guan^{4,5}  | Elizabeth A. Ainsworth^{2,3,6}  | Carl J. Bernacchi^{6,2,3} 

¹Tohoku Agricultural Research Center, National Agriculture and Food Research Organization, Morioka, Japan

²Department of Plant Biology, University of Illinois at Urbana-Champaign, Urbana, Illinois, USA

³Carl R. Woese Institute for Genomic Biology, University of Illinois at Urbana-Champaign, Urbana, Illinois, USA

⁴College of Agricultural, Consumer and Environmental Sciences, University of Illinois at Urbana-Champaign, Urbana, Illinois, USA

⁵National Center for Supercomputing Applications, University of Illinois at Urbana-Champaign, Urbana, Illinois, USA

⁶Global Change and Photosynthesis Research Unit, USDA-ARS, Urbana, Illinois, USA

Correspondence

Etsushi Kumagai, Tohoku Agricultural Research Center, National Agricultural and Food Research Organization (NARO), Morioka, Iwate 0200198, Japan.
Email: ekumagai@affrc.go.jp

Present address

Etsushi Kumagai, Institute of Agro-Environmental Sciences, NARO, Tsukuba, Ibaraki 3058604, Japan

Funding information

U.S. Department of Agriculture; the Global Change and Photosynthesis Research Unit of the USDA Agricultural Research Service; the National Institute of Food and Agriculture, Grant/Award Number: 2017-67013-26253

Abstract

Traditional gas exchange measurements are cumbersome, which makes it difficult to capture variation in biochemical parameters, namely the maximum rate of carboxylation measured at a reference temperature ($V_{\text{cmax}25}$) and the maximum electron transport at a reference temperature ($J_{\text{max}25}$), in response to growth temperature over time from days to weeks. Hyperspectral reflectance provides reliable measures of $V_{\text{cmax}25}$ and $J_{\text{max}25}$; however, the capability of this method to capture biochemical acclimations of the two parameters to high growth temperature over time has not been demonstrated. In this study, $V_{\text{cmax}25}$ and $J_{\text{max}25}$ were measured over multiple growth stages during two growing seasons for field-grown soybeans using both gas exchange techniques and leaf spectral reflectance under ambient and four elevated canopy temperature treatments (ambient+1.5, +3, +4.5, and +6°C). Spectral vegetation indices and machine learning methods were used to build predictive models for $V_{\text{cmax}25}$ and $J_{\text{max}25}$, based on the leaf reflectance. Results showed that these models yielded an R^2 of 0.57–0.65 and 0.48–0.58 for $V_{\text{cmax}25}$ and $J_{\text{max}25}$, respectively. Hyperspectral reflectance captured biochemical acclimation of leaf photosynthesis to high temperature in the field, improving spatial and temporal resolution in the ability to assess the impact of future warming on crop productivity.

KEYWORDS

climate change, *Glycine max*, high-throughput phenotyping, leaf nitrogen content, machine learning regression

1 | INTRODUCTION

Global mean surface air temperature is projected to continue increasing, in the range of an additional 1.0–5.7°C, by the end of this century (IPCC, 2021). These temperature increases are likely to

threaten global food security by negatively affecting the yields of major crops, including wheat, maize, rice, and soybean (Zhao et al., 2017). Given the linkage between photosynthesis, growth, and yield (Long, Zhu, Naidu, & Ort, 2006), assessing the impact of future warming on crop yield requires understanding and quantifying the

degree to which leaf photosynthesis will respond to high temperature.

The potential photosynthetic rate (A) of C_3 crops is determined by the maximum rate of carboxylation by Rubisco (V_{cmax}) and/or the maximum rate of electron transport (J_{max}) (Long & Bernacchi, 2003). These parameters, together with a biochemically-based photosynthesis model (Farquhar, Caemmerer, & Berry, 1980), are used widely to understand crop photosynthetic performance at leaf to ecosystem scales under current and future climates (e.g., Bagley et al., 2015). Thermal acclimation of leaf photosynthesis is defined as a shift in the temperature response curve of A , which shows an increase with temperature to a thermal optimum followed by a decline thereafter (Sage & Kubien, 2007). Biochemical processes linked with thermal acclimation include (a) V_{cmax} and J_{max} measured at a reference temperature (25°C; $V_{\text{cmax}25}$ and $J_{\text{max}25}$) and (b) temperature responses of both V_{cmax} and J_{max} , indicating changes in activation and deactivation energies (Hikosaka, Ishikawa, Borjigidai, Muller, & Onoda, 2006; Sage & Kubien, 2007). The acclimation responses of $V_{\text{cmax}25}$ and $J_{\text{max}25}$ to variation in growth temperature have been widely investigated, including for herbaceous species (Bunce, 2000; Cai et al., 2020), conifer trees (Medlyn, Loustau, & Delzon, 2002), and deciduous trees (Aspinwall et al., 2016). Despite these previous studies, uncertainty exists regarding the extent to which temperature variation over a growing season impacts $V_{\text{cmax}25}$ and $J_{\text{max}25}$.

Understanding photosynthetic responses of field crops to increasing temperatures requires warming experiments under natural field conditions to represent plant responses under typical growing season conditions. Infrared heating array systems have increasingly been used to investigate the long-term effect of elevated canopy temperature on leaf photosynthesis on crops, including soybean (Ruiz-Vera et al., 2013), wheat (Cai et al., 2020; Wall, Kimball, White, & Ottman, 2011) and rice (Cai et al., 2020). The combined effects of elevated canopy temperature (3.5°C above ambient) and elevated CO_2 concentration, $[\text{CO}_2]$ (200 $\mu\text{mol mol}^{-1}$ above ambient) on $V_{\text{cmax}25}$ and $J_{\text{max}25}$ of soybean during the growing seasons showed that $V_{\text{cmax}25}$ did not change, whereas $J_{\text{max}25}$ decreased, with elevated temperature when averaged over the whole season (Rosenthal et al., 2014). However, the effects of elevated temperature varied significantly among growth stages and between years. Shorter-term (72 hr) but higher intensity (6°C) canopy warming in field-grown soybeans that simulated heat waves found that high temperature during flowering stages significantly increased $V_{\text{cmax}25}$ but did not change $J_{\text{max}25}$ (Siebers et al., 2015). On the other hand, heat waves during the late reproductive stage decreased both parameters (Siebers et al., 2015). These studies compared photosynthetic thermal acclimation between control plots and plots heated to a single heating set point above ambient. Since no experiments have addressed responses of crops over a range of increased growth temperature treatments, an experimental design will be required to assess thresholds of acclimation over various temperature treatments.

Traditional approaches using gas exchange systems to determine $V_{\text{cmax}25}$ and $J_{\text{max}25}$ (e.g., Long & Bernacchi, 2003) are time-consuming and labour-intensive. Given the degree of variation in A based on a

range of environmental conditions, both temporally and spatially resolved measurements of $V_{\text{cmax}25}$ and $J_{\text{max}25}$ are required to precisely assess the impact of warming on crop productivity. While traditional gas exchange techniques have proven effective in understanding photosynthetic responses to imposed treatments, they are not suitable to measure these parameters at the spatiotemporal scales, which are needed to understand the linkage between imposed treatments and environmental variation over a wide range of developmental stages. Proximal sensing of leaf optical properties has been identified as a promising high-throughput phenotyping technique (e.g., Silva-Perez et al., 2018) that can potentially overcome this bottleneck. Measurements of hyperspectral reflectance are rapid, taking only a few seconds, and therefore can be utilized to obtain high spatiotemporal resolution data in field experiments. Spectral vegetation indices (SVIs) based on the reflectance ratio in the visible (VIS, 400–700 nm) to the near-infrared wavelength (NIR, 700–1,300 nm) have been developed to measure V_{cmax} and J_{max} in several species (Stylinski et al., 2000; Wang, Iio, & Kakubari, 2008). Additionally, hyperspectral reflectance information in VIS, NIR, and short-wave infrared (SWIR, 1300–2,500 nm) regions combined with the partial least squares regression (PLSR) (Wold, Sjostrom, & Eriksson, 2001) has been used previously to predict V_{cmax} and J_{max} in aspen and cottonwood (Serbin, Dillaway, Kruger, & Townsend, 2012), soybean (Ainsworth, Serbin, Skoneczka, & Townsend, 2014), poplar (Barnes et al., 2017), wheat (Silva-Perez et al., 2018), and tobacco (Meacham-Hensold et al., 2019). Machine learning regressions other than PLSR such as ridge regression (RR) (Hoerl & Kennard, 1970), least absolute shrinkage and selection operator regression (LASSO) (Tibshirani, 1996), and support vector machine regression (SVR) (Cortes & Vapnik, 1995) were coupled with reflectance measurements for plant phenotyping research (Garriga et al., 2017; Li et al., 2019). Recently, Fu, Meacham-Hensold, Guan, and Bernacchi (2019) also applied PLSR, SVR, LASSO, and other methods (artificial neural network, random forest, and Gaussian process regressions) and compared the predictive accuracy for V_{cmax} and J_{max} from hyperspectral reflectance in wild and transgenic tobacco with a range of photosynthetic capacity. However, since the predictive performance of SVIs and machine learning methods can vary significantly depending on species, plant growth stages, and environment conditions (e.g., Wang et al., 2019), there is considerable uncertainty whether this approach is accurate enough to measure biochemical acclimation of $V_{\text{cmax}25}$ and $J_{\text{max}25}$ to elevated growth temperature.

$V_{\text{cmax}25}$ and $J_{\text{max}25}$ are based on photosynthetic components such as Rubisco and thylakoid membrane proteins within chloroplasts, which account for a significant portion of leaf N. Changes in $V_{\text{cmax}25}$ and $J_{\text{max}25}$ due to thermal acclimation have been accompanied by similar directional changes in leaf N content (Cai et al., 2020; Scafaro et al., 2017). However, changes in $V_{\text{cmax}25}$ and $J_{\text{max}25}$ do not necessarily coincide with that in leaf N content, indicating that the N-partitioning into photosynthetic and non-photosynthetic components changes in response to high temperature (Cai et al., 2020; Scafaro et al., 2017). In some cases, thermal acclimation also changes N-partitioning among photosynthetic components and the ratio of

$J_{\max 25}$ to $V_{\max 25}$ (Kromdijk & Long, 2016; Onoda, Hikosaka, & Hirose, 2005). Previous studies showed that PLSR coefficients of leaf N content, $V_{\max 25}$, and $J_{\max 25}$ had similar patterns in deciduous temperate trees, suggesting that the reflectance-based predictions of $V_{\max 25}$ and $J_{\max 25}$ are dominated by their relationships to leaf N content (Dechant, Cuntz, Vohland, Schulz, & Doktor, 2017). However, given the discrepancy between changes in $V_{\max 25}$, $J_{\max 25}$ and leaf N content in response to high growth temperature, spectral-based predictions of $V_{\max 25}$ and $J_{\max 25}$ might be independent of leaf N content. However, to our knowledge, there is a lack of information about this.

Soybean (*Glycine max*) is the fourth most important crop globally, with approximately 40% of world production in the Midwestern United States. High temperature is one of the environmental factors that impact leaf photosynthetic capacity and seed yield of soybean in the Midwestern US (Rosenthal et al., 2014; Ruiz-Vera et al., 2013; Siebers et al., 2015). In this study, $V_{\max 25}$ and $J_{\max 25}$ were measured from traditional gas exchange techniques, and leaf spectral reflectance were measured over multiple growth stages for soybeans under ambient and four elevated canopy temperature treatments (ambient+1.5, +3, +4.5, and +6°C) using infrared heating arrays under field conditions in central Illinois, USA over two growing seasons. The main objective of the study was to develop and evaluate leaf spectroscopy models for predicting photosynthetic biochemical acclimation to various degrees of warming. Specifically, the following questions were addressed: (a) Does the degree and direction of biochemical acclimations of $V_{\max 25}$ and $J_{\max 25}$ to warming vary seasonally in field-grown soybean?; (b) What are the differences in accuracy and interpretability (contribution of specific spectral bands) for predicting biochemical acclimation of $V_{\max 25}$ and $J_{\max 25}$ to warmer growth temperature from leaf spectra among SVIs, PLSR, RR, LASSO, and SVR?; (c) Are the spectral-based measures for biochemical acclimations of $V_{\max 25}$ and $J_{\max 25}$ to warmer growth temperature dependent on the leaf N content?

2 | MATERIALS AND METHODS

2.1 | Experimental site

The experiment was conducted on soybean (*Glycine max*) at the Soybean Free Air Concentration Enrichment (SoyFACE) research facility located at the University of Illinois in Urbana-Champaign, IL, USA (40°2'30.49"N, 88°13'58.80"W, 230 m above sea level) during the 2018 and 2019 growing seasons. The field is tile-drained and managed by conventional agronomic practices. Two commercial cultivars were planted in 0.38-m row spacing at approximately 43 seeds m⁻². Cultivars were chosen based on maturity group, with one adapted to the central Illinois growing region where SoyFACE is located and the other adapted to Southern regions of the state of Illinois. Seeding date was May 17, 2018 (DOY138) and May 31, 2019 (DOY152) (Table 1). The experiment consisted of two and four blocks in 2018 and 2019, respectively, each block consisting of one unheated (ambient temperature, AMB) and two heated plots. The heated plots were equipped

TABLE 1 Planting and measurement dates and climatic variables in the study years

Year	2018	2019
Mean air temperature ^a (°C) July–August	23.2	23.5
Sum Precipitation ^a (mm) July–August	240.0	146.8
Canopy temperature ^b (°C)		
Ambient (AMB)	22.4	21.9
AMB + 1.5°C	23.9 (1.5) ^c	23.9 (2.0)
AMB + 3°C	25.2 (2.8)	24.8 (2.9)
AMB + 4.5°C	25.8 (3.4)	26.0 (4.1)
AMB + 6°C	27.1 (4.6)	27.3 (5.4)
Planting date (DOY)	138	152
Measurement data (DOY)	192 (R2) ^d	210 (R3)
	213 (R3)	238 (R5)
	236 (R5)	

^aWeather data were recorded at Willard Airport weather station (<http://mrcc.isws.illinois.edu/CLIMATE>, accessed on 21 February 2020) near the experimental site.

^bCanopy temperatures of each treatment were averaged from July 1 to August 31, 2018 and from July 12 to August 31, 2019, respectively.

^cValues between parentheses were the difference between ambient and heated treatments.

^dStage numbers in parentheses are based on the definition in Fehr, Caviness, Burmood, and Pennington (1971). R2: full flowering; R3: beginning of pod filling; R5: beginning of seed filling.

with infrared heating arrays as modified from Kimball (2005) and fully described in Ruiz-Vera et al. (2013). Using a proportional-integral-differential feedback controlled dimmer system coupled with infrared heating arrays, the crop canopy was warmed during daytime and nighttime throughout the growing seasons to four targeted warming levels (+1.5, +3.0, +4.5, and +6.0°C) above the AMB plot. In the 2018 season, one block consisted of an AMB, AMB + 1.5°C, and AMB + 6.0°C plot and the other an AMB, AMB + 3.0°C, and AMB + 4.5°C plot. In 2019, two blocks each consisted of an AMB, AMB + 1.5°C, and AMB + 6.0°C plot, and the other two blocks had an AMB, AMB + 3.0°C, and AMB + 4.5°C plot. Canopy temperature in each plot was measured using infrared radiometers (SI-111, Apogee Instruments, Logan, UT, USA) connected to data loggers (CR1000, Campbell Scientific, Logan, UT, USA). The heater output was automatically adjusted every 5 s to control canopy temperature and data were averaged and stored over 10 min intervals. The heated area of each plot was approximately 7 m². In both seasons, the AMB and heated plots covered a width of six rows of plants (0.38-m row spacing). Each plot was further divided with plantings of two cultivars. Leaf gas exchange and leaf hyperspectral (400–2,500 nm) reflectance of two leaves (Sub-samples 1 and 2) per cultivar were measured in each plot five times throughout the two seasons [July 10 (DOY192), July 31 (DOY213) and August 23 (DOY236) in 2018 and July 28 (DOY 210) and August 25 (DOY238) in 2019, Table 1 and Figure 1], covering the reproductive stages from R2 (full flowering) to R5 (beginning of seed filling) based on the definition by Fehr et al. (1971).

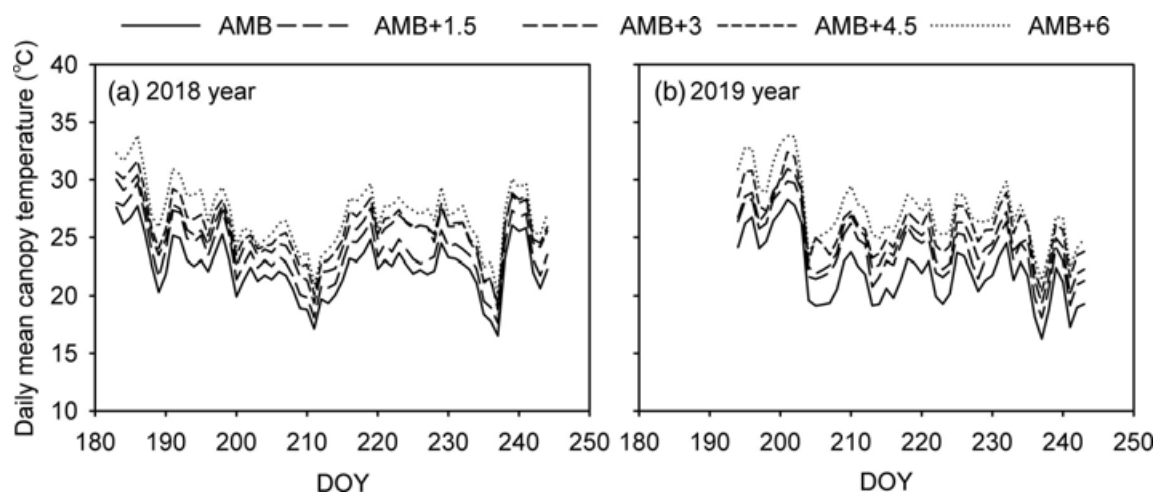


FIGURE 1 Daily mean canopy temperature at each temperature treatment from July to August of the 2018 and 2019 growing seasons. AMB, AMB + 1.5, AMB + 3, AMB + 4.5, and AMB + 6 indicate Ambient, 1.5°C above AMB, 3°C above AMB, 4.5°C above AMB, and 6°C above AMB, respectively. DOY means day of year

Air temperature and precipitation data during the two seasons were obtained from a nearby weather station located 1 km west of the experimental site (<http://mrcc.isws.illinois.edu/CLIMATE/>). Air temperature from July to August in 2018 was relatively similar to 2019, but total precipitation during July–August was higher in 2018 (Table 1). During the two seasons, the infrared heating system successfully elevated canopy temperature across a wide range from 1.5 to 5.4°C above the AMB plots (Table 1 and Figure 1).

2.2 | Leaf gas exchange measurements

We determined V_{cmax} and J_{max} from A vs. intercellular $[\text{CO}_2]$ (C_i) curves using an open gas exchange system (LI-6800, LI-COR, Lincoln, NE, USA). At predawn, the petioles of two uppermost fully expanded leaves per cultivar in each plot were excised and immediately submerged in tubes filled with water. Samples were transported to the measurement room at the SoyFACE farm and petioles were cut under water and remained submerged until measurements were complete. For several minutes before measurement, leaves were pre-treated to high light condition. Leaves were placed in the cuvette and allowed to reach steady-state photosynthesis at $400 \mu\text{mol mol}^{-1} [\text{CO}_2]$ at a saturating light of $1700 \mu\text{mol m}^{-2} \text{s}^{-1}$ and relative humidity of $\sim 65\%$. The $[\text{CO}_2]$ in the cuvette was changed stepwise in the following order: 400, 300, 250, 175, 100, 50, 400, 600, 800, $1,000 \mu\text{mol mol}^{-1}$. When steady state was achieved, A and C_i were recorded. A total of 10 data points were collected for each leaf, which were then fitted to the biochemical model of photosynthesis of Farquhar et al. (1980) to solve for V_{cmax} , J_{max} , and dark respiration rate (R_d), according to Long and Bernacchi (2003). During measurements, the cuvette temperature was controlled at 25°C . Since the mean leaf temperature was $28.4 \pm 1.3^\circ\text{C}$ (s.d.), V_{cmax} , J_{max} , and R_d normalized to 25°C ($V_{\text{cmax}25}$, $J_{\text{max}25}$, and R_{d25}) were calculated using temperature functions of Bernacchi, Singsaas, Pimentel, and Long (2001) and

Bernacchi et al. (2003). Mesophyll conductance to CO_2 was not estimated, thus $V_{\text{cmax}25}$ and $J_{\text{max}25}$ are apparent values.

2.3 | Leaf reflectance

Reflectance measurements were collected on the same two excised leaves per cultivar in each plot that were used for photosynthetic gas exchange measurements. Immediately following measurement of gas exchange, we measured leaf spectral reflectance from 400 to 2,500 nm using a full-range spectroradiometer (Fieldspec4, ASD, Boulder, MO, USA), with spectral resolution of 3 nm within 400–1,000 nm and 8 nm within 1,000–2,500 nm. All measurements were made on the adaxial surface using a leaf clip attached to a fiber optic probe with an internal and calibrated light source. The relative reflectance of each sample was determined from the measurement of leaf radiance divided by the radiance of a 99% reflective white standard (Spectralon, Labsphere Inc., North Dutton, NH, US). Six reflectance spectra were recorded using the leaf clip in different regions of the same leaf and then averaged to give a mean spectrum per leaf. Before averaging the six spectra collected from a single leaf, a splice correction was applied to spectroscopy data to ensure continuous data across the detectors. Data were interpolated to provide 1-nm bandwidths using the FieldSpectra package in R (Serbin, Singh, McNeil, Kingdon, & Townsend, 2014). Due to noise in the regions below 500 nm and above 2,400 nm, the spectral range for building predictive models was limited to 500–2,400 nm.

2.4 | Leaf N content

Immediately following reflectance measurements, three 2.01 cm^2 leaf disks were destructively sampled from each leaf and dried until constant mass, then weighed to determine leaf mass per area (LMA , g m^{-2}). Disks

were ground to a fine powder, and N content per mass (N_{mass} , mg g^{-1}) was determined by an elemental analyzer (Costech 4010; Costech Analytical Technologies, Valencia, CA, USA). Leaf N content per unit leaf area was calculated as the product of LMA and N_{mass} .

2.5 | Model building and testing

Small-waveband spectral vegetation indices (SVIs) such as CF690 (Dobrowski, Pushnik, Zarco-Tejada, & Ustin, 2005, Table S1), the normalized difference spectral vegetation indices (NDSI), and machine learning regression techniques, all described below, were applied to compare predictive accuracy for photosynthetic biochemical acclimation to warming environments. It should be emphasized here that in order to test whether the spectral reflectance can capture changes in biochemical model parameters with thermal acclimation, we combined data from five temperature conditions, including both the current and future warming environments, built several regression models, and compared their accuracy. The dataset from Sub-sample 1 of each cultivar for each plot under different DOYs throughout the two seasons was used as model building dataset ($n = 67$) to ensure that complete set of genotypes, temperature regimes, and DOYs were present in both training and test datasets. The remaining dataset from Sub-sample 2 was used only as a testing dataset ($n = 64$) to validate spectral models.

2.5.1 | Published spectral vegetation indices (SVIs)

Several SVIs have been proposed for estimating plant physiological status as chlorophyll (Chl), the xanthophyll cycle pigments, leaf water content, and Chl fluorescence, which potentially relates to leaf photosynthetic capacity (e.g., Richardson, Duigan, & Berlyn, 2002). For the comprehensive evaluation, 19 major SVIs (Table S1) were included in a comparison of predictive accuracy in the model building phase. A simple linear regression model was created based on the relationship of V_{cmax25} , J_{max25} , and leaf N content with published SVIs, and then the coefficient of determination (R^2) was determined in the model building phase.

2.5.2 | Normalized difference spectral index (NDSI) map approach

We applied the NDSI map to explore optimal indices for assessment of V_{cmax25} , J_{max25} , and leaf N content using hyperspectral data (500–2,400 nm) (Inoue et al., 2016). NDSI is calculated using the following equation:

$$\text{NDSI}(x, y) = (y - x) / (x + y) \quad (1)$$

where x and y are reflectance (R_i and R_j) values at i and j nm over the entire hyperspectral region. The NDSI map is created as a contour map of statistical indicators, such as R^2 , between the target attribute

and NDSIs. The optimum NDSI with the highest R^2 was selected, and linear regression models were built based on the relationship of V_{cmax25} , J_{max25} , and leaf N content with NDSIs. The regression of coefficient and intercept of each model were then used to calculate validation statistics for the testing dataset.

2.5.3 | Machine learning regressions

Before training each regression model, the original data of objective variables (V_{cmax25} , J_{max25} , and leaf N content) and explanatory variables (hyperspectral reflectance) of samples were standardized by the following equation:

$$z = (\text{Raw} - \text{Mean}) / \text{Std} \quad (2)$$

where z refers to the standardized value, Raw is the raw value of variables, Mean is the mean of variables, and Std is the standard deviation of variables. This pre-processing could ensure that the absolute value of the regression coefficient is a direct measure of variable importance while the coefficient shows a positive and a negative value (Li et al., 2019; Wold et al., 2001).

Four linear regression methods were used to reduce the multicollinearity problem for hyperspectral data without losing the information contributed by individual wavebands. PLSR reduces the dimensionality of the data by constructing a few principle components known as latent variables (LV). PLSR produces a set of LVs that take into consideration the values of the objective and explanatory variables simultaneously (Wold et al., 2001). RR works similar to ordinary least square regression but performs regularization by minimizing the residual sum of squares subject to the coefficient's sum of squares being non-constant (Hoerl & Kennard, 1970). This regularization is controlled using a tuning parameter (λ). LASSO performs both variable selection and regularization by minimizing the residual sum of squares subject to the sum of the absolute value of the coefficients being less than a constant (Tibshirani, 1996). In building a model with high dimensional data, LASSO regression can shrink some of the regression coefficients towards zero as the complexity parameter (λ) increases to improve the prediction accuracy. SVR is a method derived from the support vector machine (SVMs) (Cortes & Vapnik, 1995). This method mathematically transfers the regression problem into a feature space of higher dimensionality than the original data space. In this space of higher dimensionality, the regression function is parameterized to find a solution for which none of the residuals exceeds a given threshold, ε . When any residual below ε is accepted, the total of residuals exceeding ε represents the cost of the solution. The method uses a kernel function for the transfer to higher dimensionality and considers only those samples close to the margin defined by ε , which becomes the support vectors. In the present study, we used the ε -regression form of SVM and the linear kernel function in combination with a grid search for the optimization of cost parameter (C) and ε .

In this experiment, the analysis of PLSR, RR, LASSO, and SVR was carried out using the functions of `plsregss`, `ridge`, `lasso`, and `fitrsvm` in

Matlab (Mathworks, Natick, MA, USA), respectively. The optimal number of hyperparameters (LV of PLSR, λ of RR, λ of LASSO, and C and ϵ of SVR) was determined using a grid search with a five-fold cross validation to find the minimum root mean square errors for prediction to prevent overfitting. The optimum number was used to build the final model. The regression coefficients of four models were applied to the leaf spectroscopy data from the test dataset for V_{cmax25} , J_{max25} , and leaf N content.

2.5.4 | Comparison among the predictive models

To evaluate the predictive accuracy of spectral models using optimum NDSI, PLSR, RR, LASSO, and SVR in the model testing phase, we used statistical indicators such as R^2 , the relative error for prediction (REP), and the discrepancy of slope (DS). REP represents the percentage of the root mean square errors in prediction (Silva-Perez et al., 2018), defined by the following equation:

$$\text{REP}(\%) = 100 \times \left[\frac{1}{n} \sum_{i=1}^n (y_i - \hat{y}_i)^2 \right]^{0.5} / \bar{y} \quad (3)$$

where y_i and \hat{y}_i are measured and predicted traits, n is the number of samples in the dataset, and \bar{y} is the mean of the measured values of traits.

The discrepancy of the slope of regression line between measured and predicted values from unity (DS; Inoue et al., 2016) is calculated as follows:

$$\text{DS} = |1 - s| \quad (4)$$

where s is the slope of the regression line between measured and predicted data. Consequently, these three indicators represent the overall scattering including bias, sensitivity (slope), and linearity of the model, respectively (Inoue et al., 2016).

2.6 | Statistical analysis

To investigate whether acclimation of V_{cmax25} , J_{max25} , R_{d25} , and leaf N content to growth temperature occurred in field-grown soybean and whether the degree of acclimation depended on growth stages (DOYs), linear regression was applied based on the relationships of leaf photosynthetic biochemical parameters with seasonal canopy temperature in different DOYs during the two seasons. The seasonal canopy temperature was defined as the average from the preceding 15 days, according to Borjigidai et al. (2006) and Cai et al. (2020). We pooled data of two cultivars for the analysis because identifying the difference between cultivars was not our focus. We compared the responses of leaf photosynthesis attributes to seasonal canopy temperature for different growth stages (DOY) by means of analysis of covariance (ANCOVA). Firstly, we used separate-slope ANCOVA to test for slope differences. Whenever the DOY \times canopy temperature

interaction term was not significant, we continued the analysis using a common-slope model.

To investigate the dependencies of V_{cmax25} and J_{max25} to leaf N content, data were first analysed using simple linear regression. Because we observed the low value of R^2 (0.05) for the V_{cmax25} to leaf N content relationship, the data were further analysed using two-segmental piecewise regression. All statistical procedures were performed in SIGMAPLOT software (Systat Software, Inc., San Jose, CA, USA).

3 | RESULTS

3.1 | J_{max25} and leaf N content decreased with increasing canopy temperature later in growth

Figure 2 shows the relationships between V_{cmax25} and J_{max25} determined from gas exchange measurements (A-Ci curves) and leaf N content against canopy temperature at various DOYs over two growing seasons. The results showed that slopes or intercepts of regression lines for V_{cmax25} , J_{max25} , and leaf N versus mean canopy temperature differed significantly among DOYs in both seasons (Figure 2). There were no trends of V_{cmax25} with an increase of canopy temperature in all DOYs except for DOY236 (R5) in 2018 when V_{cmax25} increased with canopy temperature (Figure 2a,d). J_{max25} decreased with increasing canopy temperature at DOY213 (R3), DOY236 (R5) in 2018 and DOY238 (R5) in 2019 (Figure 2b,e), which was accompanied by significant decreases of leaf N content with increasing canopy temperature (Figure 2c, f). However, less pronounced responses of J_{max25} and leaf N content to canopy temperature were observed in the first DOY during the two seasons. The results showed that there was no difference of slope and intercept of R_{d25} to canopy temperature relationship among DOYs in the two seasons (Figure S1). There were no trends of R_{d25} with increasing canopy temperature in all DOYs, but on DOY213 (R3) in 2018 R_{d25} decreased significantly with canopy temperature. Values of V_{cmax25} and J_{max25} from different DOY were closely associated with leaf N content (Figure 3a,b). When all data were pooled, there was a significant linear relationship between J_{max25} and leaf N content with a relatively high R^2 (0.48). On the other hand, applying a two-segmental piecewise regression for V_{cmax25} and leaf N content showed a higher R^2 (0.28) than the simple linear regression ($R^2 = 0.05$). V_{cmax25} increased linearly with an increase of leaf N content up to 2.0 g m^{-2} and did not increase above this breakpoint.

3.2 | Machine learning regressions predict parameters better than optimum NDSI and published SVIs

The reflectance spectra obtained under ambient and four high-temperature conditions showed the typical pattern of green leaves (Figure 4a). The properties of reflectance spectra varied largely within and across the temperature treatments as well as DOYs over seasons.

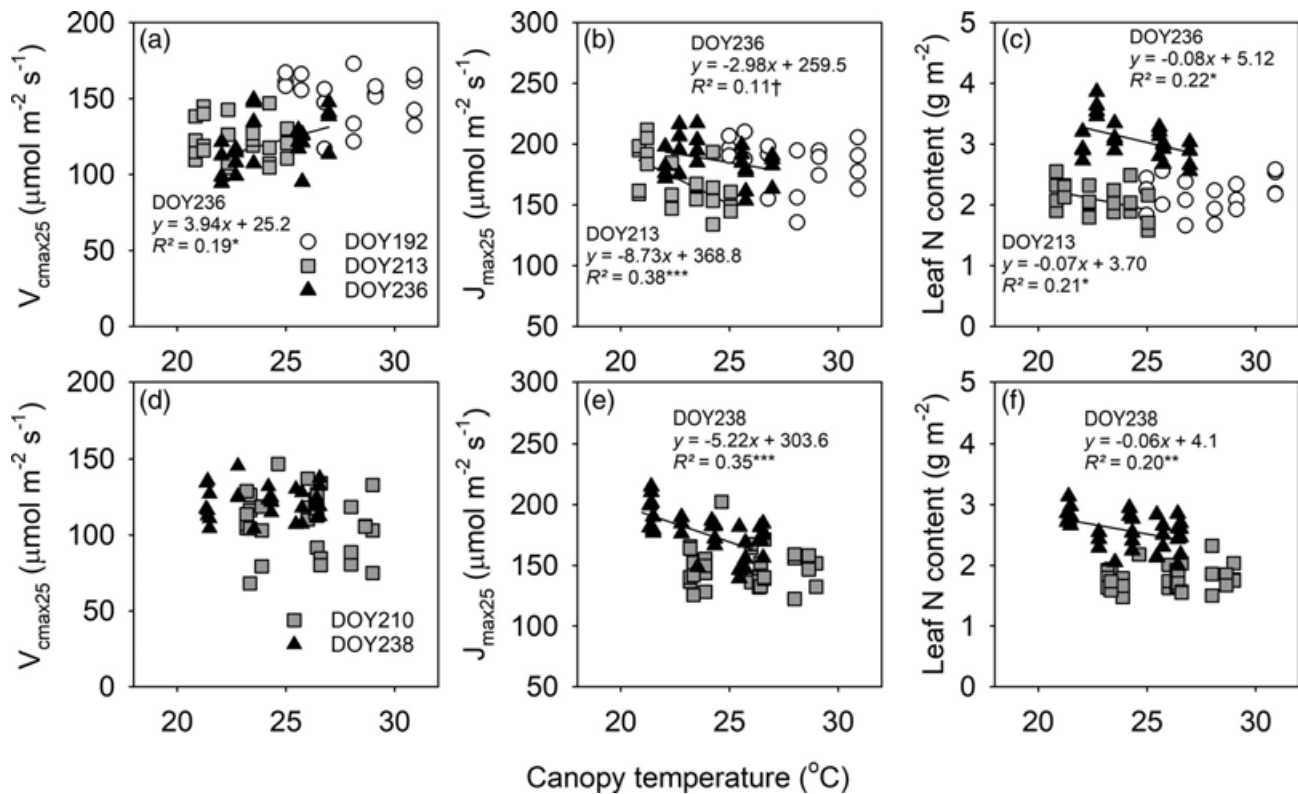
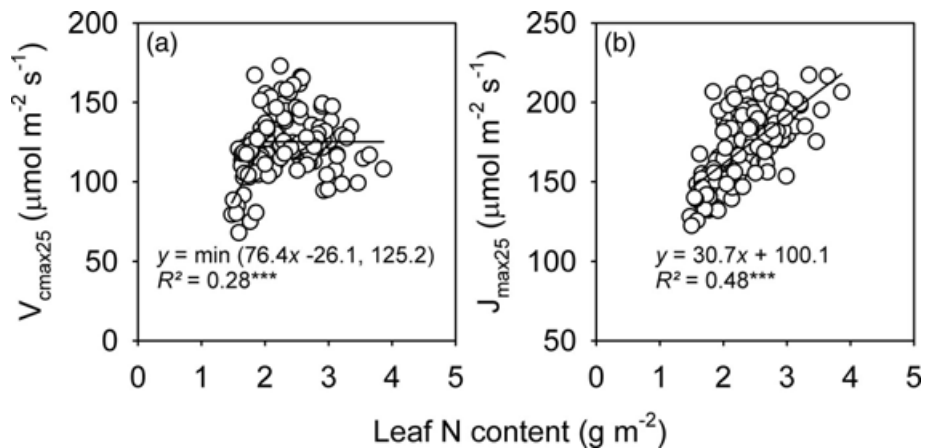


FIGURE 2 Values of maximum carboxylation rate of Rubisco at 25°C ($V_{\text{cmax}25}$) (a, d) and maximum electron transport rate at 25°C ($J_{\text{max}25}$) (b, e) and leaf nitrogen (N) content (c, f) of soybean at various day of year (DOY) in response to canopy temperature in the infrared heating arrays in the 2018 and 2019 growing seasons. Based on analysis for covariance (ANCOVA) of DOY effects with canopy temperature, the slope of the relationship of $V_{\text{cmax}25}$ and leaf N content with canopy temperature was differed significantly among DOYs ($p = .051$ and $.031$, respectively) in the 2018 season. The slope of the relationships of canopy temperature with $J_{\text{max}25}$ was not significantly different among DOYs ($p = .103$), but the intercept was different among DOYs ($p < .001$) in the 2018 season. The slope of the relationship of $J_{\text{max}25}$ and leaf N content with canopy temperature differed significantly between DOYs ($p < .05$ and $< .05$, respectively) in the 2019 season. The slope of the relationships of canopy temperature with $V_{\text{cmax}25}$ was not significantly different between DOYs ($p = .719$), but the intercept was different between DOYs ($p < .05$) in the 2019 season. The line was fitted for data from each DOY and represented significant linear regressions (p values, $\dagger < .1$, $* < .05$, $** < .01$, $*** < .001$)

FIGURE 3 Values of maximum carboxylation rate of Rubisco at 25°C ($V_{\text{cmax}25}$) (a) and maximum electron transport rate at 25°C ($J_{\text{max}25}$) (b) in relation to leaf nitrogen (N) content of soybean in the infrared heating arrays. The line was fitted for all data from the two years and represented significant linear regressions (p values, $*** < .001$)



The coefficient of variation of the reflectance was the largest in the SWIR2 region (17%), followed by the VIS region (15%) and the SWIR1 region (10%) (Figure 4b).

Next, accuracy was compared for several regression models that were built to predict parameters from reflectance obtained under

future warming environments. Figure S2 shows contour plots of NDSI R^2 values for $V_{\text{cmax}25}$, $J_{\text{max}25}$, and leaf N content obtained from the model building dataset. In the map of NDSI- $V_{\text{cmax}25}$ (Figure S2A), the area with the highest correlation ($R^2 = 0.39$) was in the range of R1862, R1865. In the NDSI- $J_{\text{max}25}$ map (Figure S2B), the area with

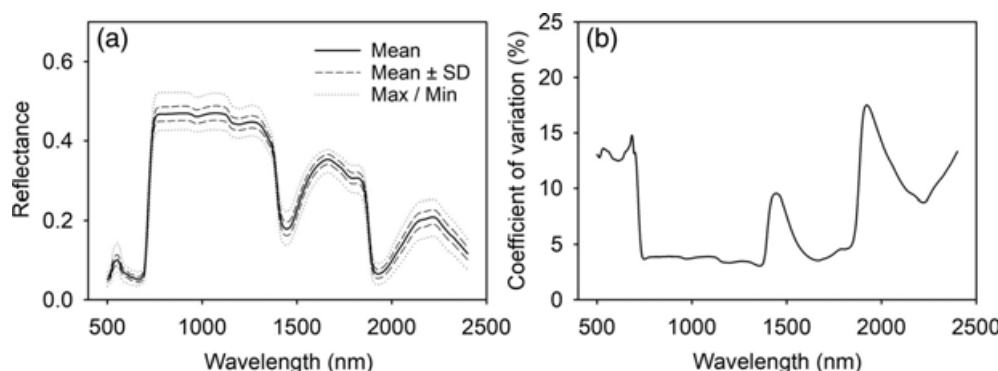


FIGURE 4 Mean, standard deviation (SD), and minimum (Max) and maximum (Min) leaf reflectance for all leaves of soybean used in this study (a) and the coefficient of variation (%) across the full spectra (b)

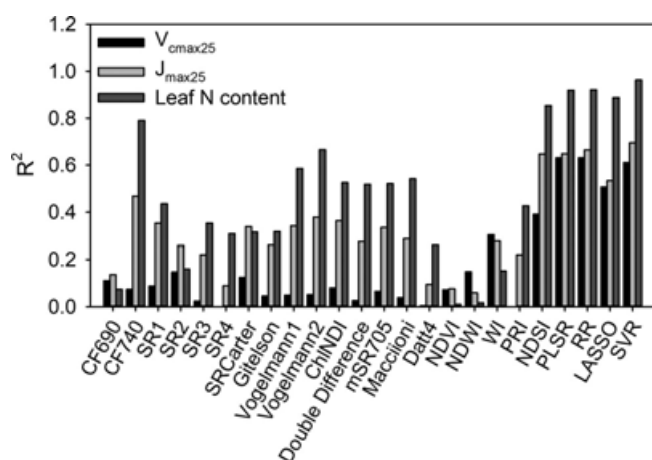


FIGURE 5 Comparison of the determination coefficients (R^2) among the spectral models of maximum carboxylation rate of Rubisco at 25°C (V_{cmax25}), maximum electron transport rate at 25°C (J_{max25}), and leaf nitrogen (N) content from published spectral vegetation indices (SVIs) and normalized difference spectral index (NDSI) explored in this study and machine learning regression in the model building phase. NDSI indicates NDSI (1862, 1865) for V_{cmax25} , NDSI (1814, 2170) for J_{max25} , and NDSI (1351, 1708) for leaf N content, respectively

the highest correlation ($R^2 = 0.65$) was near R1814, R2170. In the NDSI-leaf N content map (Figure S2C), the most significant peak for NDSI was found at R1351, R1708. Figure 5 shows the comparison of R^2 among the spectral models for V_{cmax25} , J_{max25} , and leaf N content from the published SVIs, optimum NDSIs explored here, and machine learning regression in the model building phase. The models using 19 published SVIs yielded the lower R^2 , ranging from 0.01 (SR3) to 0.30 (WI) for V_{cmax25} , from 0.06 (NDWI) to 0.47 (CF740) for J_{max25} , and from 0.01 (NDVI) to 0.79 (CF740) for leaf N content, than the models of optimum NDSIs did. Four machine learning regression models for V_{cmax25} yielded the higher R^2 from 0.51 (LASSO) to 0.63 (PLSR and RR) compared with optimum NDSIs in the model building phase. R^2 of machine learning regressions for predicting J_{max25} , except for LASSO, was similar to optimum NDSI. The four models for leaf N content ($R^2 = 0.88$ – 0.96) outperformed the model using optimum NDSI ($R^2 = 0.86$).

3.3 | Difference in prediction accuracies among the four machine learning regressions in model test phase was marginal

The accuracy of spectral models of optimum NDSI and four machine learning regressions to predict the variations of V_{cmax25} , J_{max25} , and leaf N content under ambient and four high-temperature conditions in the model test phase was compared using the values of linearity (R^2), robustness (REP), and sensitivity (DS) in Table 2. The relationships between measured values and predictive values in all spectral models were summarized in Figures S3, S4, and S5. Overall, the differences of R^2 and REP were marginal among the models for V_{cmax25} , J_{max25} , and leaf N content. For the prediction of V_{cmax25} , RR yielded the highest R^2 of 0.65 and the lowest REP of 9.5%, followed by PLSR with R^2 of 0.63 and REP of 9.8%, and SVR with R^2 of 0.61 and REP of 10.0%. NDSI (1862, 1865) and LASSO showed lower R^2 (0.57 and 0.56, respectively) and higher REP (10.8 and 10.6%, respectively) than RR, PLSR, and SVR. For predicting J_{max25} , RR outperformed with the highest R^2 of 0.58 and the lowest REP of 8.4%, followed by PLSR with R^2 of 0.56 and REP of 8.6%, and NDSI (1814, 2170) model with R^2 of 0.55 and REP of 8.8%. When compared with these models, the values of R^2 and REP were lower in SVR ($R^2 = 0.52$, REP = 8.9%) and higher in LASSO ($R^2 = 0.48$, REP = 9.4%). The best model for predicting leaf N content based on R^2 and REP was achieved by SVR ($R^2 = 0.94$, REP = 5.4%), followed by RR ($R^2 = 0.92$, REP = 6.4%), PLSR ($R^2 = 0.92$, REP = 6.5%), LASSO ($R^2 = 0.88$, REP = 7.8%), and NDSI (1351, 1708) ($R^2 = 0.86$, REP = 8.5%). The DS (from 1:1 line in Figures S3, S4, and S5) for V_{cmax25} and leaf N content was smaller in PLSR, RR, and SVR than in NDSI and LASSO. The DS for J_{max25} was the smallest in SVR, followed by NDSI, PLSR, RR, and LASSO in order of smaller to larger. The larger DS in NDSI and LASSO for V_{cmax25} and leaf N content and LASSO for J_{max25} indicates poor sensitivity.

3.4 | Wavelength bands existed that contributed to predictions in machine learning models

Standardized regression coefficients were determined to compare the relative significance of different wavebands in each machine learning

TABLE 2 Comparison of predictive accuracy of spectral models for assessment maximum carboxylation rate of Rubisco at 25°C ($V_{\text{cmax}25}$), maximum electron transport rate at 25°C ($J_{\text{max}25}$), and leaf nitrogen (N) content of soybean in the model testing phase

Variables	Coefficient of determination (R^2)				
	NDSI ^a	PLSR	RR	LASSO	SVR
$V_{\text{cmax}25}$	0.57	0.63	0.65	0.56	0.61
$J_{\text{max}25}$	0.55	0.56	0.58	0.48	0.52
Leaf N content	0.86	0.92	0.92	0.88	0.94
	Relative error for prediction (REP, %)				
	NDSI ^a	PLSR	RR	LASSO	SVR
$V_{\text{cmax}25}$	10.8	9.8	9.5	10.6	10.0
$J_{\text{max}25}$	8.8	8.6	8.4	9.4	8.9
Leaf N content	8.5	6.5	6.4	7.8	5.4
	Discrepancy of slope (DS)				
	NDSI ^a	PLSR	RR	LASSO	SVR
$V_{\text{cmax}25}$	0.53	0.23	0.29	0.51	0.28
$J_{\text{max}25}$	0.39	0.39	0.40	0.64	0.31
Leaf N content	0.17	0.10	0.11	0.20	0.06

Note: Models were built on training dataset ($n = 67$, Sub-sample 1) of the experimental data and used to predict the remaining dataset ($n = 64$, Sub-sample 2).
Abbreviations: LASSO, least absolute shrinkage and selection operator; PLSR, partial least square regression; RR, ridge regression; SVR, support vector machine regression.
^aNDSI indicates NDSI (1862, 1865) for $V_{\text{cmax}25}$, NDSI (1814, 2170) for $J_{\text{max}25}$, and NDSI (1351, 1708) for leaf N content, respectively.

regression model for predicting $V_{\text{cmax}25}$, $J_{\text{max}25}$, and leaf N content under ambient and four warming treatments (Figures S6, S7, and S8). For predicting $V_{\text{cmax}25}$, the patterns of standardized regression coefficients for PLSR were similar to RR and SVR (Figure S6). PLSR coefficients across the spectra for $J_{\text{max}25}$ were similar to RR, but somewhat different from SVR (Figure S7). PLSR and RR coefficients for leaf N content showed similar patterns, but SVR coefficients showed different patterns across the spectra (Figure S8). Most LASSO coefficients for all photosynthetic attributes shrunk to zero, resulting in the selection of wavebands for the trait prediction. The LASSO model selected six, ten, and three bands for $V_{\text{cmax}25}$, $J_{\text{max}25}$, and leaf N content, respectively (Figure S6, S7, and S8). All wavebands had specific positive or negative values for PLSR, RR, and SVR coefficients. In these three regression models, the wavebands that influenced where absolute coefficient values were greater than the mean absolute value from all spectra. As a result, all four models for predicting $V_{\text{cmax}25}$ selected five wavebands of 699, 700, 746, 747, and 748 nm across the red edge (Figure 6a). All four models for $J_{\text{max}25}$ selected three bands of 2,168, 2,169, and 2,170 nm in the SWIR2 (Figure 6b). Six bands of 649, 650, and 728 nm in the Chl bands (640 and 660 nm) and 994 nm in the NIR and 2,277 and 2,278 nm in the SWIR2 were selected by all models for predicting leaf N content (Figure 6c).

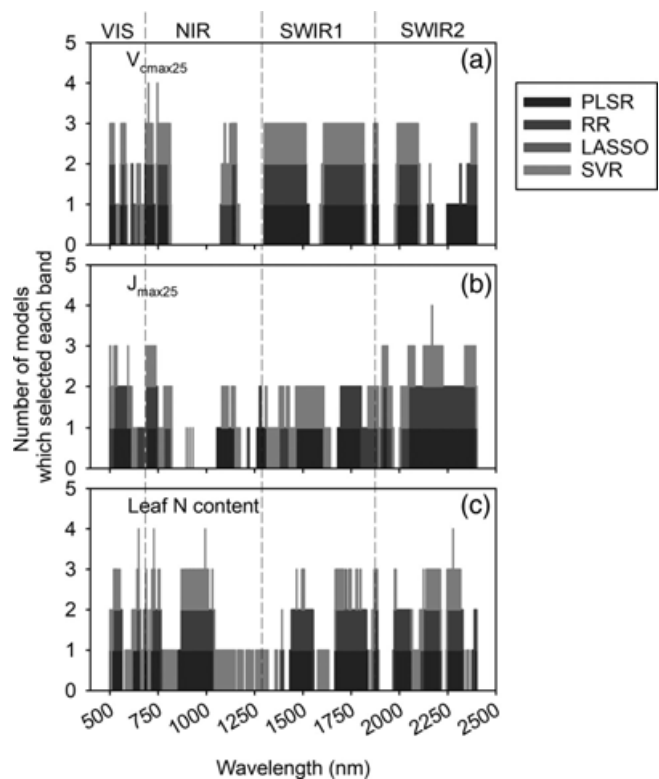


FIGURE 6 Number of spectral models for maximum carboxylation rate of Rubisco at 25°C ($V_{\text{cmax}25}$) (a), maximum electron transport rate at 25°C ($J_{\text{max}25}$) (b) and leaf nitrogen (N) content (c) which selected each band within the visible (VIS), near-infrared (NIR), short-wave infrared 1 (SWIR1), and short-wave infrared 2 (SWIR2) spectral regions. For PLSR, RR, SVR, all spectral bands had each coefficient, and therefore we selected the bands with the absolute values of coefficient greater than the mean of the absolute values from all coefficients and considered to influence the trait prediction

4 | DISCUSSION

Although photosynthetic thermal acclimation includes changes in a variety of physiological and biochemical processes, this study focused on biochemical acclimation ($V_{\text{cmax}25}$, $J_{\text{max}25}$, etc.) to high temperature. The present study addressed seasonal variation in biochemical acclimations for field-grown soybean across a wide range of growth temperature conditions that simulate gradual warming. The results showed that the decrease of $J_{\text{max}25}$ in response to warmer temperature at the R5 stage was consistent between two seasons. This provided direct evidence of the stage-dependent biochemical acclimation to high temperature, as discussed in Section 4.1. We further developed NDSI, PLSR, RR, LASSO, and SVR-based models for predicting biochemical acclimation to high temperature from leaf spectra during the whole season and compared the predictive accuracy among these models. There was no difference in the accuracy for predicting the variations of $V_{\text{cmax}25}$, $J_{\text{max}25}$, and leaf N content among PLSR, RR, LASSO, and SVR. The interpretability of each model was discussed in Section 4.2. We also tested whether the spectral-based predictions

for biochemical acclimations of $V_{\text{cmax}25}$ and $J_{\text{max}25}$ to high temperature depended on leaf N content. The results suggested that spectral-based predictions of $V_{\text{cmax}25}$ and $J_{\text{max}25}$ and leaf N content were not necessarily dependent, as discussed in Section 4.3.

4.1 | Biochemical acclimation of $V_{\text{cmax}25}$ and $J_{\text{max}25}$ to high temperature and dependency on leaf N content

Acclimation responses of photosynthetic biochemical parameters to growth temperature for field-grown soybeans were quantified at multiple growth stages across a wide range of canopy temperatures from ambient to approximately 5°C above ambient. The results showed that the decrease of $J_{\text{max}25}$ in response to warming at the R5 stage was consistent between two seasons, but not in the earlier stages (R2 and R3). (Figure 2b,e). Rosenthal et al. (2014) reported that a 3.5°C increase in canopy temperature throughout the growing season decreased mean $J_{\text{max}25}$ of soybean over many growing seasons, but the effect varied among growth stages and seasons. The results suggested that $J_{\text{max}25}$ of soybean could acclimate to warming, but this biochemical acclimation depended on the growth stage. On the other hand, $V_{\text{cmax}25}$ showed a less pronounced response to canopy temperature increase during the two seasons, with an exception that $V_{\text{cmax}25}$ increased with canopy temperature at the R5 stage (DOY236) in 2018 (Figure 2a,d). The lack of change of $V_{\text{cmax}25}$ with heating was also reported by Rosenthal et al. (2014). At the current atmospheric $[\text{CO}_2]$, A in herbaceous C_3 plants is mainly Rubisco-limited (Rogers & Humphries, 2000), which is determined by $V_{\text{cmax}25}$. The lack of observed effects of warmer temperature on A measured at 400 $\mu\text{mol mol}^{-1} \text{CO}_2$ is consistent with a lack of detectable changes in $V_{\text{cmax}25}$ for all treatments in this study (data not shown). In other words, the temperature range tested in this study had no effect on A at the current $[\text{CO}_2]$.

V_{cmax} is strongly related to Rubisco content and/or activation state (Onoda et al., 2005). However, J_{max} is determined with a complex series of reactions involving many proteins integrated into the thylakoid membrane in the chloroplast and many enzymes involved in the regeneration of RuBP (Farquhar et al., 1980). Rubisco, thylakoid membrane, and enzymes involved in RuBP regeneration account for a large proportion of leaf N. Therefore, strong and positive relationships between leaf N content per unit area and $V_{\text{cmax}25}$ and $J_{\text{max}25}$ exists in many species such as rice (Hasegawa et al., 2016), wheat (Cai et al., 2020), and temperate deciduous tree species (Dechant et al., 2017). The present study confirmed a significant and linear relationship between leaf N content and $J_{\text{max}25}$ when combined between the two seasons (Figure 3b), which agreed with previous studies (Dechant et al., 2017; Cai et al., 2020). This suggests that variations of leaf N content are partially related to seasonal dependence of biochemical acclimation of $J_{\text{max}25}$ to warmer temperature. In contrast, in this study, we did not observe any change in $V_{\text{cmax}25}$ or in leaf N content due to elevated temperature in most growth stages (Figure 2). In addition, this study confirmed a linear-plateau relationship between leaf N

content and $V_{\text{cmax}25}$ when all data were pooled (Figure 3a). In this regression equation, $V_{\text{cmax}25}$ did not increase when leaf N content was above $\sim 2.0 \text{ g m}^{-2}$. The samples with leaf N content above 2.0 g m^{-2} corresponded to approximately 70% of the total sample. Therefore, it can be concluded that treatment-induced changes in leaf N content were independent of changes in $V_{\text{cmax}25}$. A linear-plateau relationship between leaf N content and $V_{\text{cmax}25}$ has also been observed in rice (Hasegawa et al., 2016). Other studies showed the curvilinear relationship between the light-saturated A and leaf N content in some C_3 species (Evans, 1989; Sinclair & Horie, 1989). One of the possible explanations for this curvilinear relationship is the deactivation of Rubisco with the increase in the leaf N content as reported in apple (Cheng & Fuchigami, 2000). Leaf N content remains relatively low in young soybean plants, since there is a lag between nodule formation just after emergence and active N fixation, after which leaf N increases rapidly to a peak level around the mid-reproductive stage (e.g., Rosenthal et al., 2014). The presented results also showed that leaf N content, but not $V_{\text{cmax}25}$ was increased at the late stage during the two seasons. Recently, Sakoda, Suzuki, Fukayama, Tanaka, and Shiraiwa (2019) showed that the deactivation of Rubisco with N accumulation could result in constant light-saturated A during soybean reproduction. However, temperature acclimation was not associated with their results. The underlying cause of the linear-plateau relationship of $V_{\text{cmax}25}$ with leaf N content observed across a wide range of growth temperature in this study is unknown and should be clarified in future studies.

Djanaguiraman and Prasad (2010) reported that the decrease in leaf N content associated with leaf senescence in soybean occurs during the late reproductive stage and can be triggered or enhanced by high temperature. Rosenthal et al. (2014) also reported that a seasonal +3.5°C temperature increase by infrared heating accelerated the decline in leaf N content towards the end of the growing season (after DOY240). In general, leaf senescence in soybean occurs at the stage of completion of seed growth (Egli, Leggett, & Duncan, 1978). Since our measurements were completed by the R5 stage (Table 1), we concluded that the phenomena observed in this study are not related to leaf senescence.

4.2 | Prediction accuracy and interpretability for NDSI and machine learning regressions

The analysis of hyperspectral reflectance of leaves is currently established as a robust tool for capturing the genotypic variations of photosynthetic physiology in crop species (Ainsworth et al., 2014; Meacham-Hensold et al., 2019; Silva-Perez et al., 2018; Yendrek et al., 2017). Despite short-term temperature responses of V_{cmax} and J_{max} (not $V_{\text{cmax}25}$ and $J_{\text{max}25}$) being shown as predictable using PLSR analysis of reflectance spectra (Serbin et al., 2012), less attention has focused on predicting biochemical acclimations of $V_{\text{cmax}25}$ and $J_{\text{max}25}$ to future gradual warming. Although the existing SVIs are easy to calculate and able to predict V_{cmax} and J_{max} (Barnes et al., 2017; Styliniski et al., 2000; Wang et al., 2008), they are limited in predicting

biochemical acclimations of $V_{\text{cmax}25}$ and $J_{\text{max}25}$ in the model building phase (Figure 5). We explored the optimal NDSIs using full spectra with the goal of predicting variation in these parameters. We further compared the predictive accuracy using linearity (R^2), robustness (REP), and sensitivity (DS) among optimum NDSI and machine learning regressions (PLSR, RR, LASSO, and SVR) in the model testing phase. The present study showed that the variations of leaf N content under a wide range of increased growth temperatures could be predicted from hyperspectral reflectance with high accuracy with R^2 of 0.86–0.94, REP of 5.4–8.5%, and DS of 0.06–0.20 (Table 2). Relative to leaf N content, moderate accuracies were obtained for predicting $V_{\text{cmax}25}$ and $J_{\text{max}25}$, showing R^2 of 0.57–0.65 and 0.48–0.58, REP of 9.5–10.8% and 8.4–9.4%, and DS of 0.23–0.53 and 0.31–0.64, respectively. The greater predictive accuracy for leaf N content per unit area than $V_{\text{cmax}25}$ and $J_{\text{max}25}$ was also found in previous studies (Dechant et al., 2017; Silva-Perez et al., 2018). In the aspects of linearity, robustness, and sensitivity for predictions of $V_{\text{cmax}25}$, $J_{\text{max}25}$, and leaf N content, PLSR, RR, and SVR, which make use of all wavebands, performed better than LASSO, which selects specific wavebands (Table 2). Larger DS of LASSO compared with PLSR, RR, SVR for predicting $V_{\text{cmax}25}$ and leaf N content indicates larger residuals between the measured values and the predicted values in higher and lower ranges (the underestimates in higher range and overestimates in lower range) (Figures S3, S4, and S5). Similar trends were evident in the PLSR model prediction of V_{cmax} in wheat (Silva-Perez et al., 2018), which indicates that factors not accounted for in the models are driving variation in the traits (Fox & Weisberg, 2011). However, LASSO is valuable beyond maximizing predictive accuracy to assess the trade-off between the accuracy and interpretability. Therefore, the choice among the optimum models depends on this trade-off.

All spectral bands from 500 to 2,400 nm had positive or negative standardized regression coefficients for PLSR, RR, and SVR. A waveband was determined to be important in predictions when the coefficient's absolute value at a given waveband was greater than the mean absolute value across all wavebands (Figure 6). Predicting $V_{\text{cmax}25}$ using PLSR, RR, SVR, and LASSO showed five important wavebands across the red edge (699, 700, 746, 747, and 748 nm, Figure 6a). The red-edge region has been utilized to predict V_{cmax} (Dillen, Op de Beeck, Hufkens, Buonanduci, & Phillips, 2012) and is also heavily weighted in previous PLSR predictive model loadings (regression coefficients) (Meacham-Hensold et al., 2019; Silva-Perez et al., 2018; Yendrek et al., 2017). For predicting $J_{\text{max}25}$, all four models selected three bands (2,168, 2,169, and 2,170 nm, Figure 6b) in the SWIR2 region near the absorption features related to N and protein (2,180 nm; Curran, Kupiec, & Smith, 1997; Kumar, Schmidt, Dury, & Skidmore, 2001). The PLSR regression coefficient at 2,180 nm was more evident for prediction of $J_{\text{max}25}$ in a previous study (Dechant et al., 2017). Six bands of 649, 650, and 728 nm in the Chl bands (640 and 660 nm) and 994 nm in the NIR regions and 2,277 and 2,278 nm in the SWIR2 near the absorption features related to sugar, starch, and cellulose (990, 2,270, and 2,280 nm; Kumar et al., 2001) were selected by all models for predicting leaf N content. Thus, our approach, which combines four methods, is

appropriate since it can identify wavebands important for predicting the biochemical acclimations of $V_{\text{cmax}25}$, $J_{\text{max}25}$, and leaf N content. However, future studies should continue the exploration of optimal methods such as the ensemble band selection, which blends several machine learning regression techniques (Feilhauer, Asner, & Martin, 2015) to allow inference of contribution of important waveband for trait prediction.

Our main finding is that no improvements in the accuracy, linearity, and sensitivity for predicting $V_{\text{cmax}25}$, $J_{\text{max}25}$, and leaf N content under a wide range of increased growth temperatures were obtained by the non-PLSR methods (RR, LASSO, and SVR) (Table 2). Coast et al. (2019) also reported that SVR was comparable to PLSR for predicting dark respiration rate of wheat leaves from hyperspectral reflectance. Fu et al. (2019) also applied PLSR, SVR, LASSO, and other methods (artificial neural network, random forest, and Gaussian process regressions) to compare the predictive accuracy of hyperspectral reflectance to determine V_{cmax} and J_{max} on wild and transgenic tobacco, and showed that the difference of R^2 was relatively minor, ranging from 0.60 to 0.67 for V_{cmax} and from 0.48 to 0.56 for J_{max} .

The present study showed that the predictive accuracy of optimum NDSI (1814, 2170) for $J_{\text{max}25}$ was comparable to PLSR, RR, and SVR. The waveband of 2,170 nm was also selected by LASSO and showed the higher regression coefficients of PLSR, RR, and SVR. Unmanned aerial vehicle and satellite-mounted multispectral sensing systems have been widely used for estimation of crop traits (Duveiller, Baret, & Defourny, 2011; Zhang et al., 2019), but have not been used to predict photosynthetic capacity in smaller manipulative field experiments. This waveband could be a good candidate for the multispectral sensing-based prediction of leaf photosynthesis with high spatiotemporal resolution.

4.3 | Spectral-based predictions for biochemical acclimations of $V_{\text{cmax}25}$ and $J_{\text{max}25}$ to high temperature and dependency on leaf N content

The present study also tested whether the spectral-based predictions for biochemical acclimations of $V_{\text{cmax}25}$ and $J_{\text{max}25}$ to high temperature are dependent on leaf N content. A previous study (Dechant et al., 2017) suggested that spectrally-based predictions of V_{cmax} and J_{max} depend on their relationship with leaf N content by demonstrating that the patterns of the PLSR coefficients for each wavelength band of V_{cmax} , J_{max} , and leaf N content were similar. In contrast, the standardized regression coefficients of PLSR, RR, LASSO, and SVR showed different patterns among $V_{\text{cmax}25}$, $J_{\text{max}25}$, and leaf N content (Figures S6, S7, and S8). Furthermore, different bands of $V_{\text{cmax}25}$, $J_{\text{max}25}$, and leaf N content were selected by the optimum NDSI (Figure S2) and four machine learning regressions (Figure 6). As mentioned earlier, $V_{\text{cmax}25}$ was not necessarily dependent on leaf N content across a wide range of growth temperatures set in this study. It has been reported that the ratios of V_{cmax} and Rubisco content to leaf N content changed in response to changes in growth temperature (Scafaro et al., 2017). There have been cases of changes in N-

partitioning to photosynthetic components in response to growth temperature, resulting in changes in the ratio of J_{\max} to V_{\max} (Kromdijk & Long, 2016; Onoda et al., 2005). Although there was a linear relationship between leaf N content and $J_{\max25}$ in this study, $V_{\max25}$ and $J_{\max25}$ may be more related to Rubisco content, its activity, and thylakoid membrane protein content rather than to overall N content. Therefore, different wavelength bands may have been chosen for $V_{\max25}$ and $J_{\max25}$ and leaf N content in the five spectral-based methods in the present study. We concluded that the spectral-based predictions of $V_{\max25}$ and $J_{\max25}$ do not necessarily depend on the prediction of leaf N content. This supports the previous report that the PLSR model predicted accurately both V_{\max} and leaf N content for genetically modified tobacco expressing very low V_{\max} yet high leaf N content suggesting independent spectral-based predictions of V_{\max} and leaf N content (Meacham-Hensold et al., 2019).

4.4 | Advantages of hyperspectral reflectance measurements for assessing the impact of global warming on crops

The biochemical model of leaf photosynthesis developed by Farquhar et al. (1980) has become universal for describing the ecosystem response to environments in global land surface models. However, photosynthetic parameters such as $V_{\max25}$ and $J_{\max25}$ are generally derived for broad classes of vegetation and assumed to be constant during a growing season. Most modelling studies of ecosystem productivity under changing climate assume a constant value for these parameters throughout the growing season. Stinziano, Way, and Bauerle (2018) found that incorporating seasonal temperature acclimation of $V_{\max25}$ and $J_{\max25}$ improved the predictive accuracy of a carbon flux model to capture seasonal changes. Thus, it can be expected that the biochemical acclimation found here is a large source of uncertainty in modelling the ecosystem productivity under global warming. Bagley et al. (2015) incorporated seasonally varying $V_{\max25}$ and $J_{\max25}$ of soybean under infrared heating measured at 2-week intervals over the seasons (from Rosenthal et al., 2014) into a leaf biochemical and canopy photosynthesis model and compared the estimates with “one constant value for a growing season strategy”. They showed that canopy photosynthesis modelling with “one constant value for a growing season strategy” is likely to overestimate ecosystem productivity under full season warming. As reflectance measurements are rapid and non-destructive, this facilitates making more measurements throughout the whole season and on more leaves within the canopy. The higher-frequency (few-days interval) measurements, which are measurable using high-throughput by the methods proposed here, may reduce the uncertainty associated with photosynthetic biochemical acclimation when assessing the impact of future global warming on ecosystem productivity. Combining the higher-frequency prediction of biochemical model parameters of photosynthesis by reflectance measurements with a canopy photosynthesis model to test the uncertainty in the prediction of photosynthetic

production during a warming environment is likely to alter model outputs from “constant” or “bi-weekly” measurements, although to what extent needs to be addressed in future studies.

5 | CONCLUSION

The present study confirmed that biochemical acclimations ($J_{\max25}$ and leaf N content) occurred in the field-grown soybean under full season canopy warming, but the degree of biochemical acclimation varied seasonally with growth stages. As in many previous studies, this study also confirmed that variations of leaf N content could be predicted from hyperspectral reflectance. Compared with leaf N content, moderate accuracy was obtained for predicting $V_{\max25}$ and $J_{\max25}$. In the aspects of linearity, robustness, and sensitivity for predictions of $V_{\max25}$, $J_{\max25}$, and leaf N content, PLSR, RR, and SVR models, which make use of all wavebands, performed better than LASSO models, which instead relied on selecting specific wavebands. Therefore, there was some loss of information using methods that use waveband selection routines. However, despite having a relatively small sacrifice in accuracy, LASSO seemingly is a practical method as it selects relevant wavebands that could be related to known absorption features or previously published sensitive wavebands. Therefore, the choice among the optimum models depends on the trade-off between model accuracy and interpretability. Overall, compared with PLSR commonly used in the previous studies, no improvements in the accuracy, linearity, and sensitivity were obtained by RR, LASSO, or SVR. Hyperspectral reflectance can capture rapidly and accurately photosynthetic biochemical acclimation to increased temperature in the field, greatly enhancing our ability to assess the impact of future warming on ecosystem productivity.

ACKNOWLEDGMENTS

The authors would like to thank Evan Dracup, Katherine Meacham-Hensold, Matthew H. Siebers, Caitlin E. Moore, Peng Fu, Justin McGrath, Aidan McMahon, Jesse McGrath, and Chris Moller for help with this research. This work was supported in part by the National Institute of Food and Agriculture, USDA, under award number 2017-67013-26253 and from the Global Change and Photosynthesis Research Unit of the USDA Agricultural Research Service. E. K. was supported by the National Agricultural and Food Research Organization in Japan during a sabbatical leave. Any opinions, findings, and conclusions or recommendations expressed in this publication are those of the author(s) and do not necessarily reflect the views of the U.S. Department of Agriculture. Mention of trade names or commercial products in this publication is solely for the purpose of providing specific information and does not imply recommendation or endorsement by the U.S. Department of Agriculture. USDA is an equal opportunity provider and employer.

CONFLICT OF INTEREST

The authors declare no conflict of interest.

DATA AVAILABILITY STATEMENT

The data that supports the findings of this study are available in the supplementary material of this article.

ORCID

Etsushi Kumagai  <https://orcid.org/0000-0003-4724-489X>

Charles H. Burroughs  <https://orcid.org/0000-0001-9906-129X>

Christopher M. Montes  <https://orcid.org/0000-0002-7295-3092>

Bin Peng  <https://orcid.org/0000-0002-7284-3010>

Hyungsuk Kimm  <https://orcid.org/0000-0001-8189-0874>

Kaiyu Guan  <https://orcid.org/0000-0002-3499-6382>

Elizabeth A. Ainsworth  <https://orcid.org/0000-0002-3199-8999>

Carl J. Bernacchi  <https://orcid.org/0000-0002-2397-425X>

REFERENCES

- Ainsworth, E. A., Serbin, S. P., Skoneczka, J. A., & Townsend, P. A. (2014). Using leaf optical properties to detect ozone effects on foliar biochemistry. *Photosynthesis Research*, 119(1–2), 65–76. <https://doi.org/10.1007/s11120-013-9837-y>
- Aspinwall, M. J., Drake, J. E., Campamy, C., Varhammar, A., Ghannoum, O., Tissue, D. T., ... Tjoelker, M. G. (2016). Convergent acclimation of leaf photosynthesis and respiration to prevailing ambient temperatures under current and warmer climates in *Eucalyptus tereticornis*. *New Phytologist*, 212(2), 354–367. <https://doi.org/10.1111/nph.14035>
- Bagley, J., Rosenthal, D. M., Ruiz-Vera, U. M., Siebers, M. H., Kumar, P., Ort, D. R., & Bernacchi, C. J. (2015). The influence of photosynthetic acclimation to rising CO₂ and warmer temperatures on leaf and canopy photosynthesis models. *Global Biogeochemical Cycles*, 29(2), 194–206. <https://doi.org/10.1002/2014gb004848>
- Barnes, M. L., Breshears, D. D., Law, D. J., van Leeuwen, W. J. D., Monson, R. K., Fojtik, A. C., ... Moore, D. J. P. (2017). Beyond greenness: Detecting temporal changes in photosynthetic capacity with hyperspectral reflectance data. *PLoS One*, 12(12), 17. <https://doi.org/10.1371/journal.pone.0189539>
- Bernacchi, C. J., Pimentel, C., & Long, S. P. (2003). In vivo temperature response functions of parameters required to model RuBP-limited photosynthesis. *Plant Cell and Environment*, 26(9), 1419–1430. <https://doi.org/10.1046/j.0016-8025.2003.01050.x>
- Bernacchi, C. J., Singas, E., L., Pimentel, C., & Long, S. P. (2001). Improved temperature response functions for models of rubisco-limited photosynthesis. *Plant Cell and Environment*, 24(2), 253–259. <https://doi.org/10.1111/j.1365-3040.2001.00668.x>
- Borjigidai, A., Hikosaka, K., Hirose, T., Hasegawa, T., Okada, M., & Kobayashi, K. (2006). Seasonal changes in temperature dependence of photosynthetic rate in rice under a free-air CO₂ enrichment. *Annals of Botany*, 97(4), 549–557. <https://doi.org/10.1093/aob/mcl001>
- Bunce, J. A. (2000). Acclimation of photosynthesis to temperature in eight cool and warm climate herbaceous C-3 species: Temperature dependence of parameters of a biochemical photosynthesis model. *Photosynthesis Research*, 63(1), 59–67. <https://doi.org/10.1023/a:1006325724086>
- Cai, C., Li, G., Di, L., Ding, Y., Fu, L., Guo, X., ... Yin, X. (2020). The acclimation of leaf photosynthesis of wheat and rice to seasonal temperature changes in T-FACE environments. *Global Change Biology*, 26(2), 539–556. <https://doi.org/10.1111/gcb.14830>
- Cheng, L. L., & Fuchigami, L. H. (2000). Rubisco activation state decreases with increasing nitrogen content in apple leaves. *Journal of Experimental Botany*, 51(351), 1687–1694. <https://doi.org/10.1093/jexbot/51.351.1687>
- Coast, O., Shah, S., Ivakov, A., Gaju, O., Wilson, P. B., Posch, B. C., ... Atkin, O. K. (2019). Predicting dark respiration rates of wheat leaves from hyperspectral reflectance. *Plant Cell and Environment*, 42(7), 2133–2150. <https://doi.org/10.1111/pce.13544>
- Cortes, C., & Vapnik, V. (1995). Support-vector networks. *Machine Learning*, 20(3), 273–297. <https://doi.org/10.1007/bf00994018>
- Curran, P. J., Kupiec, J. A., & Smith, G. M. (1997). Remote sensing the biochemical composition of a slash pine canopy. *IEEE Transactions on Geoscience and Remote Sensing*, 35(2), 415–420. <https://doi.org/10.1109/36.563280>
- Dechant, B., Cuntz, M., Vohland, M., Schulz, E., & Doktor, D. (2017). Estimation of photosynthesis traits from leaf reflectance spectra: Correlation to nitrogen content as the dominant mechanism. *Remote Sensing of Environment*, 196, 279–292. <https://doi.org/10.1016/j.rse.2017.05.019>
- Dillen, S. Y., Op de Beeck, M., Hufkens, K., Buonanduci, M., & Phillips, N. G. (2012). Seasonal patterns of foliar reflectance in relation to photosynthetic capacity and color index in two co-occurring tree species, *Quercus rubra* and *Betula papyrifera*. *Agricultural and Forest Meteorology*, 160, 60–68. <https://doi.org/10.1016/j.agrformet.2012.03.001>
- Djanaguiraman, M., & Prasad, P. V. V. (2010). Ethylene production under high temperature stress causes premature leaf senescence in soybean. *Functional Plant Biology*, 37, 1071–1084. <https://doi.org/10.1071/FP10089>
- Dobrowski, S. Z., Pushnik, J. C., Zarco-Tejada, P. J., & Ustin, S. L. (2005). Simple reflectance indices track heat and water stress-induced changes in steady-state chlorophyll fluorescence at the canopy scale. *Remote Sensing of Environment*, 97(3), 403–414. <https://doi.org/10.1016/j.rse.2005.05.006>
- Duveiller, G., Baret, F., & Defourny, P. (2011). Crop specific green area index retrieval from MODIS data at regional scale by controlling pixel-target adequacy. *Remote Sensing of Environment*, 115(10), 2686–2701. <https://doi.org/10.1016/j.rse.2011.05.026>
- Egli, D. B., Leggett, J. W., & Duncan, W. G. (1978). Influence of stress on leaf senescence and N redistribution in soybeans. *Agronomy Journal*, 70, 43–47. <https://doi.org/10.2134/agronj1978.00021962007000010011x>
- Evans, J. R. (1989). Photosynthesis and nitrogen relationships in leaves of C3 plants. *Oecologia*, 78(1), 9–19. <https://doi.org/10.1007/bf00377192>
- Farquhar, G. D., Caemmerer, S. V., & Berry, J. A. (1980). A biochemical model of photosynthetic CO₂ assimilation in leaves of C3 species. *Planta*, 149(1), 78–90. <https://doi.org/10.1007/bf00386231>
- Fehr, W. R., Caviness, C. E., Burmood, D. T., & Pennington, J. S. (1971). Stage of development descriptions for soybeans, *Glycine max* (L.) Merrill. *Crop Science*, 11, 929–931. <https://doi.org/10.2135/cropsci1971.0011183X001100060051x>
- Feilhauer, H., Asner, G. P., & Martin, R. E. (2015). Multi-method ensemble selection of spectral bands related to leaf biochemistry. *Remote Sensing of Environment*, 164, 57–65. <https://doi.org/10.1016/j.rse.2015.03.033>
- Fox, J., & Weisberg, S. (2011). *An R companion to applied regression*. Los Angeles, London: SAGE.
- Fu, P., Meacham-Hensold, K., Guan, K. Y., & Bernacchi, C. J. (2019). Hyperspectral leaf reflectance as proxy for photosynthetic capacities: An ensemble approach based on multiple machine learning algorithms. *Frontiers in Plant Science*, 10, 13. <https://doi.org/10.3389/fpls.2019.00730>
- Garriga, M., Romero-Bravo, S., Estrada, F., Escobar, A., Matus, I. A., del Pozo, A., ... Lobos, G. A. (2017). Assessing wheat traits by spectral reflectance: Do we really need to focus on predicted trait-values or directly identify the elite genotypes group? *Frontiers in Plant Science*, 8, 280. <https://doi.org/10.3389/fpls.2017.00280>
- Hasegawa, T., Sakai, H., Tokida, T., Usui, Y., Yoshimoto, M., Fukuoka, M., ... Okada, M. (2016). Rice free-air carbon dioxide enrichment studies to improve assessment of climate change effects on rice agriculture. In

- J. L. Hatfield & D. Fleisher (Eds.), *Advances in agricultural systems modeling*. (pp. 45–68). Madison, WI: American Society of Agronomy, Crop Science Society of America, and Soil Science Society of America. <https://doi.org/10.2134/advagricsystmodel7.2014.0015>
- Hikosaka, K., Ishikawa, K., Borjigida, A., Muller, O., & Onoda, Y. (2006). Temperature acclimation of photosynthesis: Mechanisms involved in the changes in temperature dependence of photosynthetic rate. *Journal of Experimental Botany*, 57, 291–302. <https://doi.org/10.1093/jxb/erj049>
- Hoerl, A. E., & Kennard, R. W. (1970). Ridge regression – Biased estimation for nonorthogonal problems. *Technometrics*, 12(1), 55–67. <https://doi.org/10.1080/00401706.1970.10488634>
- Inoue, Y., Guerif, M., Baret, F., Skidmore, A., Gitelson, A., Schlerf, M., ... Oliso, A. (2016). Simple and robust methods for remote sensing of canopy chlorophyll content: A comparative analysis of hyperspectral data for different types of vegetation. *Plant Cell and Environment*, 39(12), 2609–2623. <https://doi.org/10.1111/pce.12815>
- IPCC (2021). In V. Masson-Delmotte, P. Zhai, A. Pirani, S. L. Connors, C. Péan, S. Berger, et al. (Eds.), *Climate change 2021: The physical science basis. Contribution of working group I to the sixth assessment report of the intergovernmental panel on climate change*. Cambridge: Cambridge University Press In Press.
- Kimball, B. A. (2005). Theory and performance of an infrared heater for ecosystem warming. *Global Change Biology*, 11(11), 2041–2056. <https://doi.org/10.1111/j.1365-2486.2005.01028.x>
- Kromdijk, J., & Long, S. P. (2016). One crop breeding cycle from starvation? How engineering crop photosynthesis for rising CO₂ and temperature could be one important route to alleviation. *Proceedings of the Royal Society of London B: Biological Sciences*, 283(1826), 20152578. <https://doi.org/10.1098/rspb.2015.2578>
- Kumar, L., Schmidt, K., Dury, S., & Skidmore, A. (2001). Imaging spectrometry and vegetation science. *Imaging Spectrometry: Basic Principles and Prospective Applications*, 4, 111–155.
- Li, J., Veeranampalayam-Sivakumar, A.-N., Bhatta, M., Garst, N. D., Stoll, H., Baenziger, P. S., ... Shi, Y. (2019). Principal variable selection to explain grain yield variation in winter wheat from features extracted from UAV imagery. *Plant Methods*, 15(1), 123. <https://doi.org/10.1186/s13007-019-0508-7>
- Long, S. P., & Bernacchi, C. J. (2003). Gas exchange measurements, what can they tell us about the underlying limitations to photosynthesis? Procedures and sources of error. *Journal of Experimental Botany*, 54(392), 2393–2401. <https://doi.org/10.1093/jxb/erg262>
- Long, S. P., Zhu, X. G., Naidu, S. L., & Ort, D. R. (2006). Can improvement in photosynthesis increase crop yields? *Plant Cell and Environment*, 29(3), 315–330. <https://doi.org/10.1111/j.1365-3040.2005.01493.x>
- Meacham-Hensold, K., Montes, C. M., Wu, J., Guan, K. Y., Fu, P., Ainsworth, E. A., ... Bernacchi, C. J. (2019). High-throughput field phenotyping using hyperspectral reflectance and partial least squares regression (PLSR) reveals genetic modifications to photosynthetic capacity. *Remote Sensing of Environment*, 231, 10. <https://doi.org/10.1016/j.rse.2019.04.029>
- Medlyn, B. E., Loustau, D., & Delzon, S. (2002). Temperature response of parameters of a biochemically based model of photosynthesis. I. Seasonal changes in mature maritime pine (*Pinus pinaster* Ait.). *Plant Cell and Environment*, 25(9), 1155–1165. <https://doi.org/10.1046/j.1365-3040.2002.00890.x>
- Onoda, Y., Hikosaka, K., & Hirose, T. (2005). The balance between RuBP carboxylation and RuBP regeneration: A mechanism underlying the interspecific variation in acclimation of photosynthesis to seasonal change in temperature. *Functional Plant Biology*, 32(10), 903–910. <https://doi.org/10.1071/fp05024>
- Richardson, A. D., Duigan, S. P., & Berlyn, G. P. (2002). An evaluation of noninvasive methods to estimate foliar chlorophyll content. *New Phytologist*, 153(1), 185–194. <https://doi.org/10.1046/j.0028-646X.2001.00289.x>
- Rogers, A., & Humphries, S. W. (2000). A mechanistic evaluation of photosynthetic acclimation at elevated CO₂. *Global Change Biology*, 6(8), 1005–1011. <https://doi.org/10.1046/j.1365-2486.2000.00375.x>
- Rosenthal, D. M., Ruiz-Vera, U. M., Siebers, M. H., Gray, S. B., Bernacchi, C. J., & Ort, D. R. (2014). Biochemical acclimation, stomatal limitation and precipitation patterns underlie decreases in photosynthetic stimulation of soybean (*Glycine max*) at elevated CO₂ and temperatures under fully open air field conditions. *Plant Science*, 226, 136–146. <https://doi.org/10.1016/j.plantsci.2014.06.013>
- Ruiz-Vera, U. M., Siebers, M., Gray, S. B., Drag, D. W., Rosenthal, D. M., Kimball, B. A., ... Bernacchi, C. J. (2013). Global warming can negate the expected CO₂ stimulation in photosynthesis and productivity for soybean grown in the Midwestern United States. *Plant Physiology*, 162(1), 410–423. <https://doi.org/10.1104/pp.112.211938>
- Sage, R. F., & Kubien, D. S. (2007). The temperature response of C₃ and C₄ photosynthesis. *Plant, Cell & Environment*, 30(9), 1086–1106. <https://doi.org/10.1111/j.1365-3040.2007.01682.x>
- Sakoda, K., Suzuki, S., Fukayama, H., Tanaka, Y., & Shiraiwa, T. (2019). Activation state of rubisco decreases with the nitrogen accumulation during the reproductive stage in soybean *Glycine max* (L.) Merr. *Photosynthetica*, 57(1), 231–236. <https://doi.org/10.32615/ps.2019.002>
- Scafaro, A. P., Xiang, S., Long, B. M., Bahar, N. H. A., Weerasinghe, L. K., Creek, D., ... Atkin, O. K. (2017). Strong thermal acclimation of photosynthesis in tropical and temperate wet-forest tree species: The importance of altered rubisco content. *Global Change Biology*, 23(7), 2783–2800. <https://doi.org/10.1111/gcb.13566>
- Serbin, S. P., Dillaway, D. N., Kruger, E. L., & Townsend, P. A. (2012). Leaf optical properties reflect variation in photosynthetic metabolism and its sensitivity to temperature. *Journal of Experimental Botany*, 63(1), 489–502. <https://doi.org/10.1093/jxb/err294>
- Serbin, S. P., Singh, A., McNeil, B. E., Kingdon, C. C., & Townsend, P. A. (2014). Spectroscopic determination of leaf morphological and biochemical traits for northern temperate and boreal tree species. *Ecological Applications*, 24(7), 1651–1669. <https://doi.org/10.1890/13-2110.1>
- Siebers, M. H., Yendrek, C. R., Drag, D., Locke, A. M., Acosta, L. R., Leakey, A. D. B., ... Ort, D. R. (2015). Heat waves imposed during early pod development in soybean (*Glycine max*) cause significant yield loss despite a rapid recovery from oxidative stress. *Global Change Biology*, 21(8), 3114–3125. <https://doi.org/10.1111/gcb.12935>
- Silva-Perez, V., Molero, G., Serbin, S. P., Condon, A. G., Reynolds, M. P., Furbank, R. T., & Evans, J. R. (2018). Hyperspectral reflectance as a tool to measure biochemical and physiological traits in wheat. *Journal of Experimental Botany*, 69(3), 483–496. <https://doi.org/10.1093/jxb/erx421>
- Sinclair, T. R., & Horie, T. (1989). Leaf nitrogen, photosynthesis, and crop radiation efficiency – A review. *Crop Science*, 29(1), 90–98. <https://doi.org/10.2135/cropsci1989.0011183X002900010023x>
- Stinziano, J. R., Way, D. A., & Bauerle, W. L. (2018). Improving models of photosynthetic thermal acclimation: Which parameters are most important and how many should be modified? *Global Change Biology*, 24(4), 1580–1598. <https://doi.org/10.1111/gcb.13924>
- Stylinski, C. D., Oechel, W. C., Gamon, J. A., Tissue, D. T., Miglietta, F., & Raschi, A. (2000). Effects of lifelong CO₂ enrichment on carboxylation and light utilization of *Quercus pubescens* Willd. Examined with gas exchange, biochemistry and optical techniques. *Plant Cell and Environment*, 23(12), 1353–1362. <https://doi.org/10.1046/j.1365-3040.2000.00638.x>
- Tibshirani, R. (1996). Regression shrinkage and selection via the lasso. *Journal of the Royal Statistical Society Series B-Methodological*, 58(1), 267–288. <https://doi.org/10.1111/j.2517-6161.1996.tb02080.x>
- Wall, G. W., Kimball, B. A., White, J. W., & Ottman, M. J. (2011). Gas exchange and water relations of spring wheat under full-season infrared warming. *Global Change Biology*, 17(6), 2113–2133. <https://doi.org/10.1111/j.1365-2486.2011.02399.x>

- Wang, Q., Iio, A., & Kakubari, Y. (2008). Broadband simple ratio closely traced seasonal trajectory of canopy photosynthetic capacity. *Geophysical Research Letters*, 35(7), L07401. <https://doi.org/10.1029/2008gl033619>
- Wang, Z., Townsend, P. A., Schweiger, A. K., Couture, J. J., Singh, A., Hobbie, S. E., & Cavender-Bares, J. (2019). Mapping foliar functional traits and their uncertainties across three years in a grassland experiment. *Remote Sensing of Environment*, 221, 405–416. <https://doi.org/10.1016/j.rse.2018.11.016>
- Wold, S., Sjostrom, M., & Eriksson, L. (2001). PLS-regression: A basic tool of chemometrics. *Chemometrics and Intelligent Laboratory Systems*, 58(2), 109–130. [https://doi.org/10.1016/s0169-7439\(01\)00155-1](https://doi.org/10.1016/s0169-7439(01)00155-1)
- Yendrek, C. R., Tomaz, T., Montes, C. M., Cao, Y. Y., Morse, A. M., Brown, P. J., ... Ainsworth, E. A. (2017). High-throughput phenotyping of maize leaf physiological and biochemical traits using hyperspectral reflectance. *Plant Physiology*, 173(1), 614–626. <https://doi.org/10.1104/pp.16.01447>
- Zhang, S. M., Zhao, G. X., Lang, K., Su, B. W., Chen, X. N., Xi, X., & Zhang, H. B. (2019). Integrated satellite, unmanned aerial vehicle (UAV) and ground inversion of the SPAD of winter wheat in the reviving stage. *Sensors*, 19(7), 17. <https://doi.org/10.3390/s19071485>
- Zhao, C., Liu, B., Piao, S., Wang, X., Lobell, D. B., Huang, Y., ... Asseng, S. (2017). Temperature increase reduces global yields of major crops in four independent estimates. *Proceedings of the National Academy of Sciences of the United States of America*, 114(35), 9326–9331. <https://doi.org/10.1073/pnas.1701762114>

SUPPORTING INFORMATION

Additional supporting information may be found in the online version of the article at the publisher's website.

How to cite this article: Kumagai, E., Burroughs, C. H., Pederson, T. L., Montes, C. M., Peng, B., Kimm, H., Guan, K., Ainsworth, E. A., & Bernacchi, C. J. (2022). Predicting biochemical acclimation of leaf photosynthesis in soybean under in-field canopy warming using hyperspectral reflectance. *Plant, Cell & Environment*, 45, 80–94. <https://doi.org/10.1111/pce.14204>